



*Supplement of*

## Astronomical calibration of the geological timescale: closing the middle Eocene gap

T. Westerhold et al.

Correspondence to: T. Westerhold ([tvesterhold@marum.de](mailto:tvesterhold@marum.de))

The copyright of individual parts of the supplement might differ from the CC-BY 3.0 licence.

## **Expression of precession and short-eccentricity cycles in core images**

To illustrate the possible expression of precession and short-eccentricity cycles in core images we provide two figures on Sites 702 and 1263 core data. The hierarchical expression of cyclicity or bundling of cycles is easy to recognize in the Paleocene and Maastrichtian Zumaia section (Dinarès-Turell et al., 2003; Kuiper et al., 2008; Dinarès-Turell et al., 2013; Batenburg et al., 2014; Dinarès-Turell et al., 2014). Figure S4a displays the 166 to 180 rmcd interval at Site 1263 including a 2.4 Myr minimum at approximately 168 rmcd to a more pronounced short eccentricity cyclicity below. The figure shows the individual images from two holes, 1263A and 1263B, as well as the combined (spliced) image. Slight color differences between Holes 1263A and 1263B image are related to aperture setting changes during the shipboard image acquisition. These color differences between the two holes are artifacts that cannot easily be corrected for. There is no clear expression of precession although slight changes in color may occur on decimeter level. The short eccentricity cycles appear a bit darker at  $\delta^{13}\text{C}$  minima corresponding to eccentricity maxima, similar to the observations of Lourens et al. (2005) for the early Eocene. Core images of Hole 702B (Fig. S4b) are bright white with no apparent expressions of precession or short eccentricity cycles. The figure shows Cores 702B-12X and 702B-13X, time equivalents to the 1263 images of Fig. S4a. In general, core-box images taken during ODP times (“table layout images”) suffer from severe unequal lighting. Because of this most cores are darker in the upper right corner (see 702B-12X in Fig. S4b). Both ODP cores do not show the clear cycle bundling as in some outcrops on land (Zumaia) that can be utilized for astronomical tuning.

## **Phase relationship between bulk carbon isotopes and eccentricity**

For the astronomical tuning of the bulk  $\delta^{13}\text{C}$  data from 702B and 1263 lighter (more negative)  $\delta^{13}\text{C}$  peaks are correlated to La2011 eccentricity maxima. The rationale for picking this phase relationship is based on several high profile studies, including modeling of carbon cycle and Earth’s orbit interaction (Zachos et al., 2001a; Cramer et al., 2003; Billups et al., 2004; Lourens et al., 2005; Pälike et al., 2006a; Pälike et al., 2006b; Holbourn et al., 2007; Tian et al., 2008; Russon et al., 2010; Zachos et al., 2010; Lunt et al., 2011; Ma et al., 2011; Sexton et al., 2011; Westerhold et al., 2011; Proistosescu et al., 2012; Holbourn et al., 2013; Kirtland Turner et al., 2014; Littler et al., 2014) dealing with the phase relation of  $\delta^{13}\text{C}$  and the 405-kyr orbital eccentricity cycle. All these studies show that the Pliocene to Cenozoic  $\delta^{13}\text{C}$  values in benthic and bulk deep sea carbonate reveal augmented 405-kyr cycles with minima in  $\delta^{13}\text{C}$  (lighter values) and  $\% \text{CaCO}_3$  (i.e. peaks in Fe) corresponding to eccentricity

maxima. This phase relation is also observed in the records from ODP Site 1258 (Kirtland Turner et al., 2014) and 1260 (Edgar et al., 2007) as shown herein. The  $\delta^{13}\text{C}$  cycles are consistent with a climate-carbon cycle feedback, as indicated by a relative lag in  $\delta^{13}\text{C}$  relative to  $\delta^{18}\text{O}$ . The strong 405-kyr cycle in benthic and bulk  $\delta^{13}\text{C}$  data as well as simulated  $\delta^{13}\text{C}$  results from a resonance associated with the long residence time of carbon in the ocean (Broecker and Peng, 1982; Pälike et al., 2006a; Ma et al., 2011). Periodic changes in oceanic  $\delta^{13}\text{C}$  on Milankovitch time scales are likely caused by changes in weathering induced carbon input changing the burial ratio of  $\text{CaCO}_3$  to organic carbon (Cramer et al., 2003; Ma et al., 2011). An increase in weathering intensity and riverine carbon supply will increase the burial ratio of  $\text{CaCO}_3$  to organic carbon leading to a decrease in  $\delta^{13}\text{C}$  (minima, lighter values in bulk  $\delta^{13}\text{C}$ ). During eccentricity maxima weathering intensity and nutrient supply is enhanced leading via the biosphere productivity feedback to lighter bulk  $\delta^{13}\text{C}$  values in the stable carbon isotope records. The phase lag of  $\delta^{13}\text{C}$  to eccentricity has been estimated to be in the order of 50 and 10 kyr for long and short eccentricity (Herbert, 1997; Zachos et al., 2001b; Holbourn et al., 2007; Zachos et al., 2010; Westerhold et al., 2011) in the Neogene and Paleogene. This leads to the assumption that the uncertainty in astronomical tuning presented here is in the order of less than 50 kyr. In fact the main uncertainty derives from the error in the 405-kyr eccentricity cycle in the order of 50 kyr at 56 Ma and 60 kyr at 66 Ma.

## References:

- Batenburg, S. J., Gale, A. S., Sprovieri, M., Hilgen, F. J., Thibault, N., Boussaha, M., and Orue-Etxebarria, X.: An astronomical time scale for the Maastrichtian based on the Zumaia and Sopelana sections (Basque country, northern Spain), *Journal of the Geological Society*, 10.1144/jgs2013-015, 2014.
- Billups, K., Pälike, H., Channell, J. E. T., Zachos, J. C., and Shackleton, N. J.: Astronomic calibration of the late Oligocene through early Miocene geomagnetic polarity time scale, *Earth and Planetary Science Letters*, 224, 33-44, 2004.
- Broecker, W. S., and Peng, T. H.: Tracers in the Sea, edited by: University, C., Lamont Doherty Geol. Obs. Publications, New York, 689 pp., 1982.
- Channell, J. E. T., Hodell, D. A., Singer, B. S., and Xuan, C.: Reconciling astrochronological and  $^{40}\text{Ar}/^{39}\text{Ar}$  ages for the Matuyama-Brunhes boundary and late Matuyama Chron, *Geochem. Geophys. Geosyst.*, 11, 21, 10.1029/2010GC003203 2010.
- Charles, A. J., Condon, D. J., Harding, I. C., Pälike, H., Marshall, J. E. A., Cui, Y., Kump, L., and Croudace, I. W.: Constraints on the numerical age of the Paleocene-Eocene boundary, *Geochem. Geophys. Geosyst.*, 12, Q0AA17, 10.1029/2010gc003426, 2011.
- Cramer, B. S., Wright, J. D., Kent, D. V., and Aubry, M.-P.: Orbital climate forcing of  $\delta^{13}\text{C}$  excursions in the late Paleocene - Eocene (chrons C24n-C25n), *Paleoceanography*, 18, 1097, 10.1029/2003PA000909, 2003.
- Dinarès-Turell, J., Baceta, J. I., Pujalte, V., Orue-Etxebarria, X., Bernaola, G., and Lorito, S.: Untangling the Paleocene climatic rhythm: an astronomically calibrated Early Paleocene magnetostratigraphy and biostratigraphy at Zumaia (Basque basin, northern Spain), *Earth and Planetary Science Letters*, 216, 483-500, 2003.
- Dinarès-Turell, J., Pujalte, V., Stoykova, K., and Elorza, J.: Detailed correlation and astronomical forcing within the Upper Maastrichtian succession in the Basque Basin, *Boletín Geológico y Minero*, 124, 253-282, 2013.
- Dinarès-Turell, J., Westerhold, T., Pujalte, V., Röhl, U., and Kroon, D.: Astronomical calibration of the Danian stage (Early Paleocene) revisited: Settling chronologies of sedimentary records across the Atlantic and Pacific Oceans, *Earth and Planetary Science Letters*, 405, 119-131, 10.1016/j.epsl.2014.08.027, 2014.
- Edgar, K. M., Wilson, P. A., Sexton, P. F., and Suganuma, Y.: No extreme bipolar glaciation during the main Eocene calcite compensation shift, *Nature*, 448, 908-911, 10.1038/nature06053, 2007.
- Herbert, T. D.: A long marine history of carbon cycle modulation by orbital-climatic changes, *Proc. Natl. Acad. Sci. USA*, 94, 8362-8369, 1997.
- Holbourn, A., Kuhnt, W., Schulz, M., Flores, J.-A., and Andersen, N.: Orbitally-paced climate evolution during the middle Miocene "Monterey" carbon-isotope excursion, *Earth and Planetary Science Letters*, 261, 534-550, 2007.
- Holbourn, A., Kuhnt, W., Clemens, S., Prell, W., and Andersen, N.: Middle to late Miocene stepwise climate cooling: Evidence from a high-resolution deep water isotope curve spanning 8 million years, *Paleoceanography*, 28, 2013PA002538, 10.1002/2013PA002538, 2013.
- Kirtland Turner, S., Sexton, P. F., Charles, C. D., and Norris, R. D.: Persistence of carbon release events through the peak of early Eocene global warmth, *Nature Geosci.*, 7, 10.1038/ngeo2240, 2014.

- Kuiper, K. F., Deino, A., Hilgen, F. J., Krijgsman, W., Renne, P. R., and Wijbrans, J. R.: Synchronizing Rock Clocks of Earth History, *Science*, 320, 500-504, 10.1126/science.1154339, 2008.
- Laskar, J., Fienga, A., Gastineau, M., and Manche, H.: La2010: a new orbital solution for the long-term motion of the Earth, *Astronomy and Astrophysics*, 532, A89, 10.1051/0004-6361/201116836, 2011a.
- Laskar, J., Gastineau, M., Delisle, J. B., Farrés, A., and Fienga, A.: Strong chaos induced by close encounters with Ceres and Vesta, *Astronomy and Astrophysics*, 532, L4, 10.1051/0004-6361/201117504, 2011b.
- Littler, K., Röhl, U., Westerhold, T., and Zachos, J. C.: A high-resolution benthic stable-isotope record for the South Atlantic: Implications for orbital-scale changes in Late Paleocene-Early Eocene climate and carbon cycling, *Earth and Planetary Science Letters*, 401, 18-30, 10.1016/j.epsl.2014.05.054, 2014.
- Lourens, L. J., Sluijs, A., Kroon, D., Zachos, J. C., Thomas, E., Röhl, U., Bowles, J., and Raffi, I.: Astronomical pacing of late Palaeocene to early Eocene global warming events, *Nature*, 435, 1083-1087, 10.1038/nature03814, 2005.
- Lunt, D. J., Ridgwell, A., Sluijs, A., Zachos, J., Hunter, S., and Haywood, A.: A model for orbital pacing of methane hydrate destabilization during the Palaeogene, *Nature Geosci*, 4, 775-778, 10.1038/ngeo1266, 2011.
- Ma, W., Tian, J., Li, Q., and Wang, P.: Simulation of long eccentricity (400-kyr) cycle in ocean carbon reservoir during Miocene Climate Optimum: Weathering and nutrient response to orbital change, *Geophysical Research Letters*, 38, L10701, 10.1029/2011GL047680, 2011.
- Pálike, H., Frazier, J., and Zachos, J. C.: Extended orbitally forced palaeoclimatic records from the equatorial Atlantic Ceara Rise, *Quaternary Science Reviews*, 25, 3138-3149, 2006a.
- Pálike, H., Norris, R. D., Herrle, J. O., Wilson, P. A., Coxall, H. K., Lear, C. H., Shackleton, N. J., Tripati, A. K., and Wade, B. S.: The Heartbeat of the Oligocene Climate System, *Science*, 314, 1894-1898, 10.1126/science.1133822, 2006b.
- Proistosescu, C., Huybers, P., and Maloof, A. C.: To tune or not to tune: Detecting orbital variability in Oligo-Miocene climate records, *Earth and Planetary Science Letters*, 325-326, 100-107, 10.1016/j.epsl.2012.01.022, 2012.
- Renne, P. R., Swisher, C. C., Deino, A. L., Karner, D. B., Owens, T. L., and DePaolo, D. J.: Intercalibration of standards, absolute ages and uncertainties in  $^{40}\text{Ar}/^{39}\text{Ar}$  dating, *Chemical Geology*, 145, 117-152, 1998.
- Renne, P. R., Mundil, R., Balco, G., Min, K., and Ludwig, K. R.: Joint determination of  $^{40}\text{K}$  decay constants and  $^{40}\text{Ar}^*/^{40}\text{K}$  for the Fish Canyon sanidine standard, and improved accuracy for  $^{40}\text{Ar}/^{39}\text{Ar}$  geochronology, *Geochimica et Cosmochimica Acta*, 74, 5349-5367, 10.1016/j.gca.2010.06.017, 2010.
- Rivera, T. A., Storey, M., Zeeden, C., Hilgen, F. J., and Kuiper, K.: A refined astronomically calibrated  $^{40}\text{Ar}/^{39}\text{Ar}$  age for Fish Canyon sanidine, *Earth and Planetary Science Letters*, 311, 420-426, 10.1016/j.epsl.2011.09.017, 2011.
- Russon, T., Paillard, D., and Elliot, M.: Potential origins of 400–500 kyr periodicities in the ocean carbon cycle: A box model approach, *Global Biogeochemical Cycles*, 24, GB2013, 10.1029/2009GB003586, 2010.
- Sexton, P. F., Norris, R. D., Wilson, P. A., Pálike, H., Westerhold, T., Röhl, U., Bolton, C. T., and Gibbs, S.: Eocene global warming events driven by ventilation of oceanic dissolved organic carbon, *Nature*, 471, 349-352, 10.1038/nature09826, 2011.
- Shipboard Scientific Party: Site 1263, in: Proc. ODP, Init. Repts., 208: College Station, TX (Ocean Drilling Program), edited by: Zachos, J. C., Kroon, D., Blum, P., and et al., 1-87, 10.2973/odp.proc.ir.208.104.2004, 2004.
- Tian, J., Zhao, Q., Wang, P., Li, Q., and Cheng, X.: Astronomically modulated Neogene sediment records from the South China Sea, *Paleoceanography*, 23, 10.1029/2007PA001552, 2008.
- Westerhold, T., Röhl, U., Laskar, J., Bowles, J., Raffi, I., Lourens, L. J., and Zachos, J. C.: On the duration of magnetostratigraphic C24r and C25n and the timing of early Eocene global warming events: Implications from the Ocean Drilling Program Leg 208 Walvis Ridge depth transect, *Paleoceanography*, 22, 10.1029/2006PA001322, 2007.
- Westerhold, T., Röhl, U., Raffi, I., Fornaciari, E., Monechi, S., Reale, V., Bowles, J., and Evans, H. F.: Astronomical calibration of the Paleocene time, *Palaeogeography, Palaeoclimatology, Palaeoecology*, 257, 377-403, 10.1016/j.palaeo.2007.09.016, 2008.
- Westerhold, T., and Röhl, U.: High resolution cyclostratigraphy of the early Eocene - new insights into the origin of the Cenozoic cooling trend, *Clim Past*, 5, 309-327, 10.5194/cp-5-309-2009, 2009.
- Westerhold, T., Röhl, U., McCarron, H. K., and Zachos, J. C.: Latest on the absolute age of the Paleocene-Eocene Thermal Maximum (PETM): New insights from exact stratigraphic position of key ash layers+19 and-17, *Earth and Planetary Science Letters*, 287, 412-419, 10.1016/j.epsl.2009.08.027, 2009.
- Westerhold, T., Röhl, U., Donner, B., McCarron, H. K., and Zachos, J. C.: A complete high-resolution Paleocene benthic stable isotope record for the central Pacific (ODP Site 1209), *Paleoceanography*, 26, PA2216, 10.1029/2010pa002092, 2011.
- Westerhold, T., Röhl, U., and Laskar, J.: Time scale controversy: Accurate orbital calibration of the early Paleogene, *Geochem. Geophys. Geosyst.*, 13, Q06015, 10.1029/2012gc004096, 2012.
- Zachos, J., Pagani, M., Sloan, L., Thomas, E., and Billups, K.: Trends, Rhythms, and Aberrations in Global Climate 65 Ma to Present, *Science*, 292, 686-693, 10.1126/science.1059412, 2001a.
- Zachos, J., Shackleton, N. J., Revenaugh, J. S., Pálike, H., and Flower, B. P.: Climate Response to Orbital Forcing Across the Oligocene-Miocene Boundary, *Science*, 292, 274-278, 10.1126/science.1058288, 2001b.
- Zachos, J. C., McCarron, H., Murphy, B., Röhl, U., and Westerhold, T.: Tempo and scale of late Paleocene and early Eocene carbon isotope cycles: Implications for the origin of hyperthermals, *Earth and Planetary Science Letters*, 299, 242-249, 10.1016/j.epsl.2010.09.004, 2010.

## Figure Legends

**Figure S1.** ODP Site 1263 magnetic susceptibility data (Shipboard Scientific Party, 2004) from Holes A (red), B (blue) and C (green) on the new revised composite depth. Data and core images are plotted for each hole separately. Red vertical lines are the tops and yellow vertical lines are the bases of splice sections. All magnetic susceptibility data are the instrument units raw in  $10^{-5}$ .

**Figure S2.** MTM power spectra of ODP Hole 702B bulk  $\delta^{13}\text{C}$  data from various intervals in the depth and age (magnetostratigraphy ages CK95) domain.

**Figure S3.** MTM power spectra of ODP Site 1263 bulk  $\delta^{13}\text{C}$  data from various intervals in the depth and age (magnetostratigraphy ages CK95) domain.

**Figure S4.** Close up of ODP Site 1263 and Hole 702B to illustrate the potential expression of precession and short-eccentricity cycles in core images.

**Figure S5.** Comparison of sedimentation rates for Site 1263 and Hole 702B records using the tuned, the magnetostratigraphic, the 17 405-kyr cyclo- and 18 405-kyr cyclostratigraphic age model. Bulk  $\delta^{13}\text{C}$  data (gray) and the magnetostratigraphy are also shown.

**Figure S6.** Eccentricity solutions La2010a-d (Laskar et al., 2011a) and La2011 (Laskar et al., 2011b) of the Earth (fine black line) compared to geological data to assess the positions of the 2.4 myr eccentricity cycle minima from 41 to 60 Ma. To accentuate successive minima in the eccentricity solution the amplitude modulation (AM) was extracted from the orbital solution (thick gray line). Geochemical data with a dominant eccentricity component are plotted on the stable 405-kyr cyclostratigraphic framework anchored to the ATS. Data: bulk  $\delta^{13}\text{C}$  from 1258 in light blue (Kirtland Turner et al., 2014), 1262 in bright blue (Littler et al., 2014; Zachos et al., 2010) and 1263 in dark blue (this study); benthic  $\delta^{13}\text{C}$  from 1258 in gray (Sexton et al., 2011); XRF core scanning iron (Fe) intensity data from 1262 in orange (Westerhold et al., 2007; Westerhold et al., 2008) and 1258 in red (Westerhold and Röhl, 2009). Also given is the position of the Paleocene-Eocene Thermal Maximum (PETM) (Westerhold et al., 2007) and ash -17 (Westerhold et al., 2009). Light blue bars mark the 2.4 myr eccentricity minima in the geological data. The comparison shows that none of the orbital solutions matches all of the minima in the geological records back to 60 Ma. La2011 and La2010d reproduce all minima up to 48 Ma. Therefore, for astronomical dating only these two solutions are robust back to 48 Ma. For older times only the stable 405-kyr eccentricity cycle should be utilized.

**Figure S7.** Comparison of astronomical and radio-isotopic ages for the Paleocene-Eocene Thermal Maximum (PETM) and ash -17. Gray bars mark the absolute age range for the onset of the PETM based on the age and relative distance of ash -17 with respect to the age of the Fish Canyon (FC) radiometric dating  $^{40}\text{Ar}/^{39}\text{Ar}$  standard of 28.02 (Renne et al., 1998), 28.201 (Kuiper et al., 2008), 28.305 (Renne et al., 2010), 27.93 (Channell et al., 2010), 27.89 (Westerhold et al., 2012), 28.172 (Rivera et al., 2011) and 28.10 (this study) Ma. Horizontal black lines mark the three possible options of the age range for the onset of the PETM based on the astronomically calibrated Paleocene time scale (Westerhold et al., 2008). The red bar and arrow as well as light blue bar and arrow mark the astronomically calibrated absolute age for the onset of the PETM and ash -17 consistent with the 2.4 myr minima in the La2011 orbital solution (Westerhold et al., 2012). The green bar and arrow as well as the blue bar and arrow mark the age of the onset of the PETM and ash -17 consistent with the stable 405-kyr cyclostratigraphy established in this study. The black double dot with error bar shows the age of the onset of the PETM based on a high precision radio-isotopic U/Pb age of 55.728 - 55.964 Ma from bentonite layers within the PETM interval at Spitzbergen (Charles et al., 2011). The U/Pb age and the stable 405-kyr cyclostratigraphy age of ~55.9 Ma are independent from uncertainties in the 100-kyr and 2.4 myr eccentricity cycle components and therefore the most robust age for the onset of the PETM.

**Figure S8.** Detailed graph of bulk  $\delta^{13}\text{C}$  data from 702B (red) and 1263 (black) plotted on the tuned age model. (A) Both records plotted on the same  $\delta^{13}\text{C}$  axis. Benthic foraminifers'  $\delta^{13}\text{C}$  data from Katz and Miller (1991). (B) Zoom of the 46.5 to 48.2 Ma interval plotted on a separate  $\delta^{13}\text{C}$  axes. Black lines mark lighter  $\delta^{13}\text{C}$  values at 702B at 47.23, 47.39, 47.55 and 48.08 Ma that correlate with lighter values in 1263. Note that the 47.39 and 47.55 Ma peaks at 702B are single data points and that due to the sample resolution of 20 cm at 702B in this interval transient  $\delta^{13}\text{C}$  excursions could be missed.

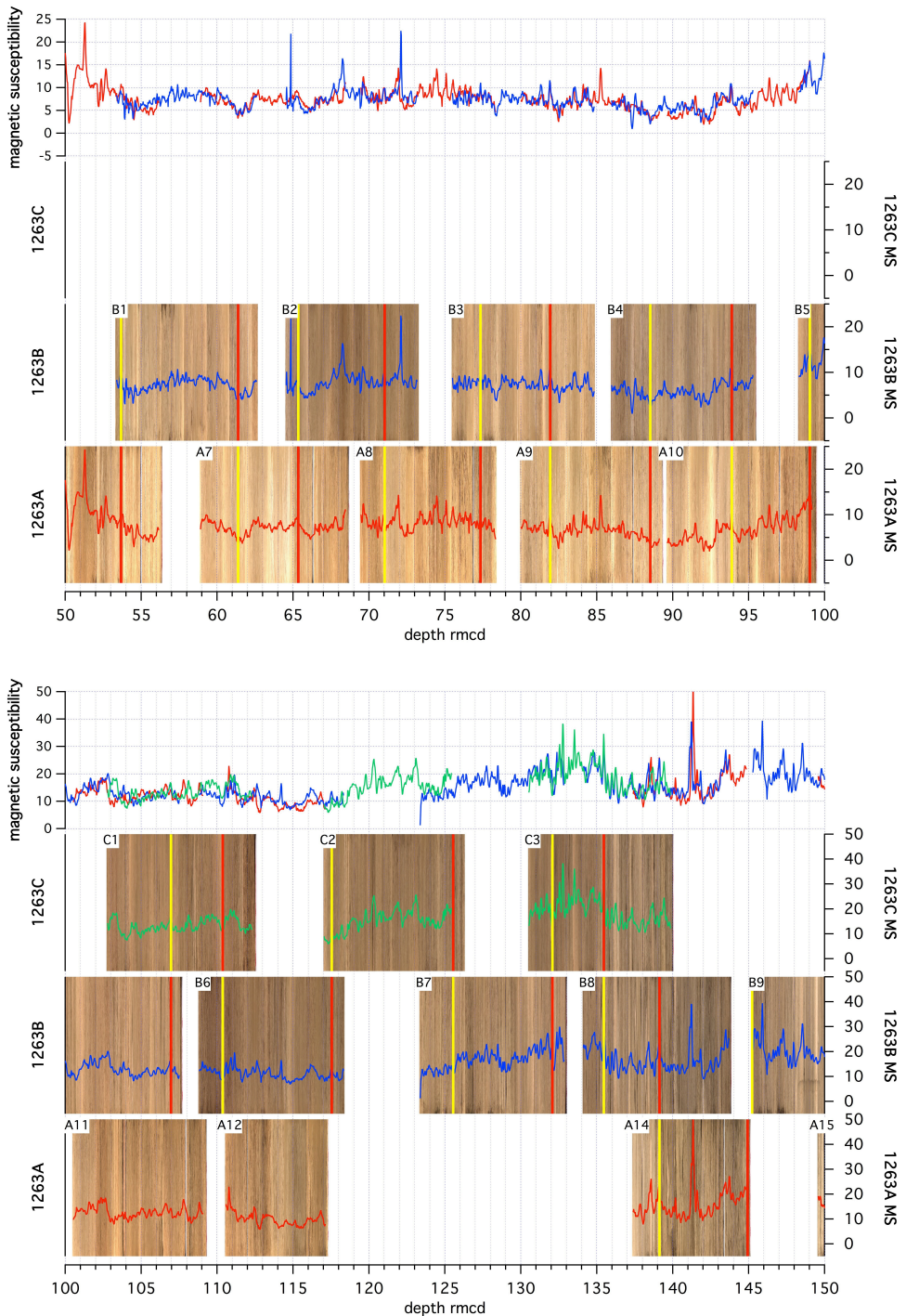


**Figure S1**

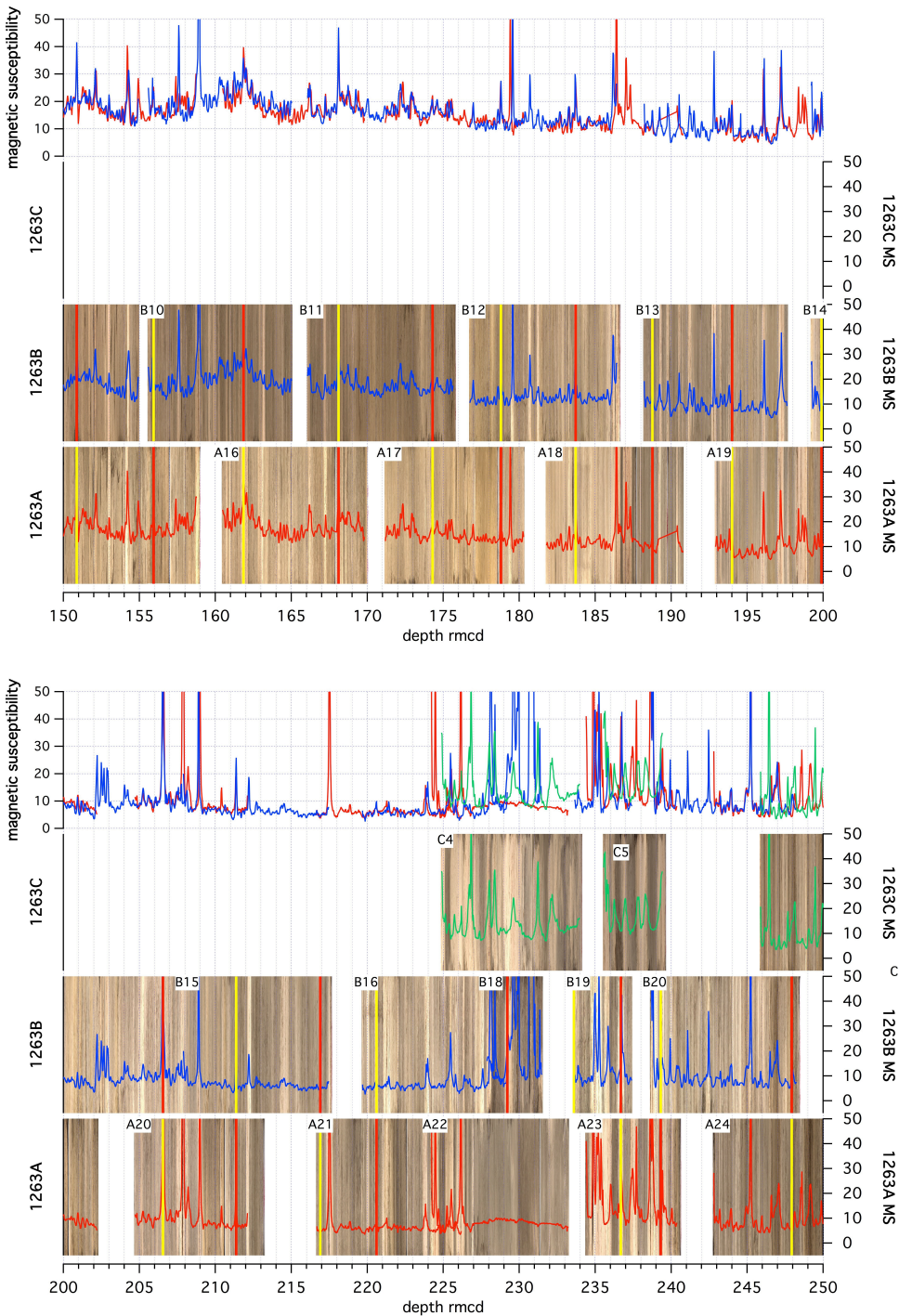


**Figure S1 - continued.**

### 702B bulk $\delta^{13}\text{C}$

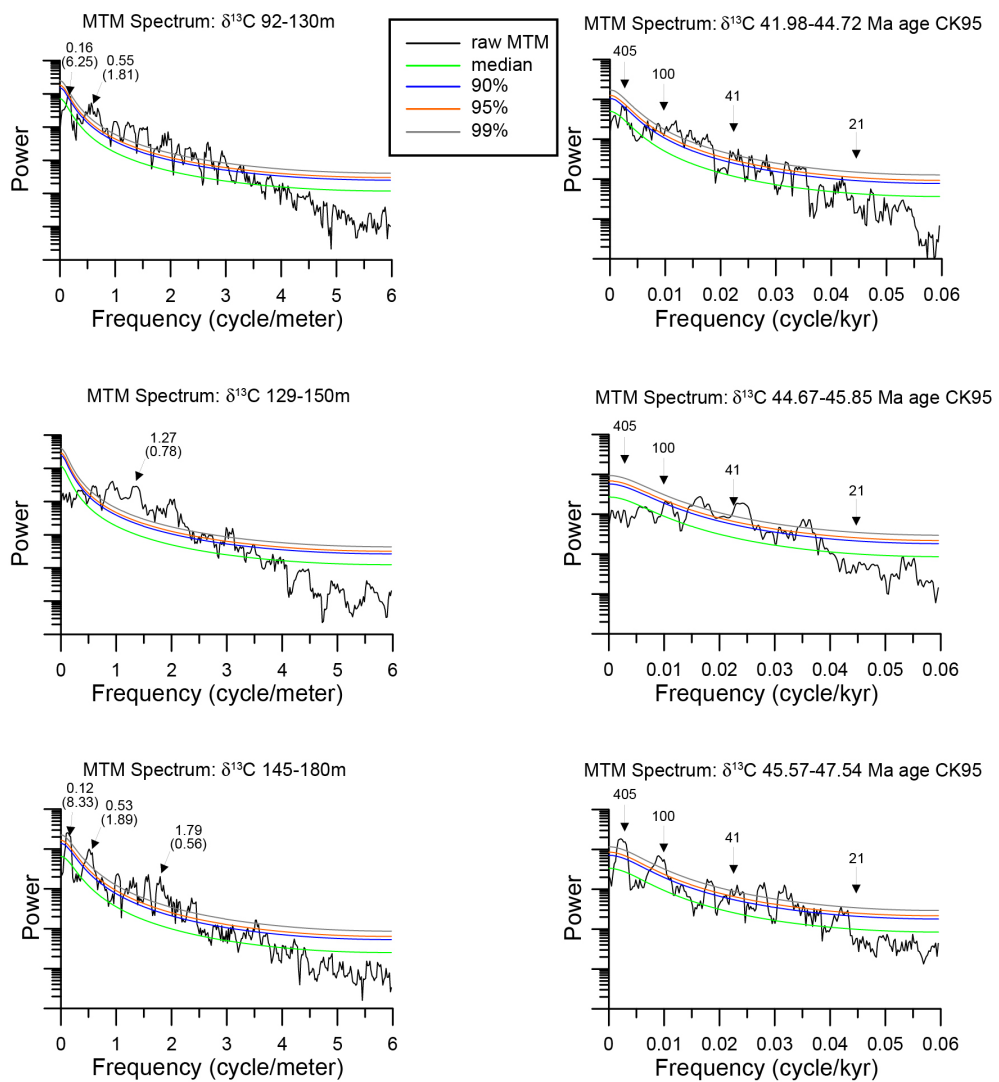


**Figure S2**

### 1263 bulk $\delta^{13}\text{C}$

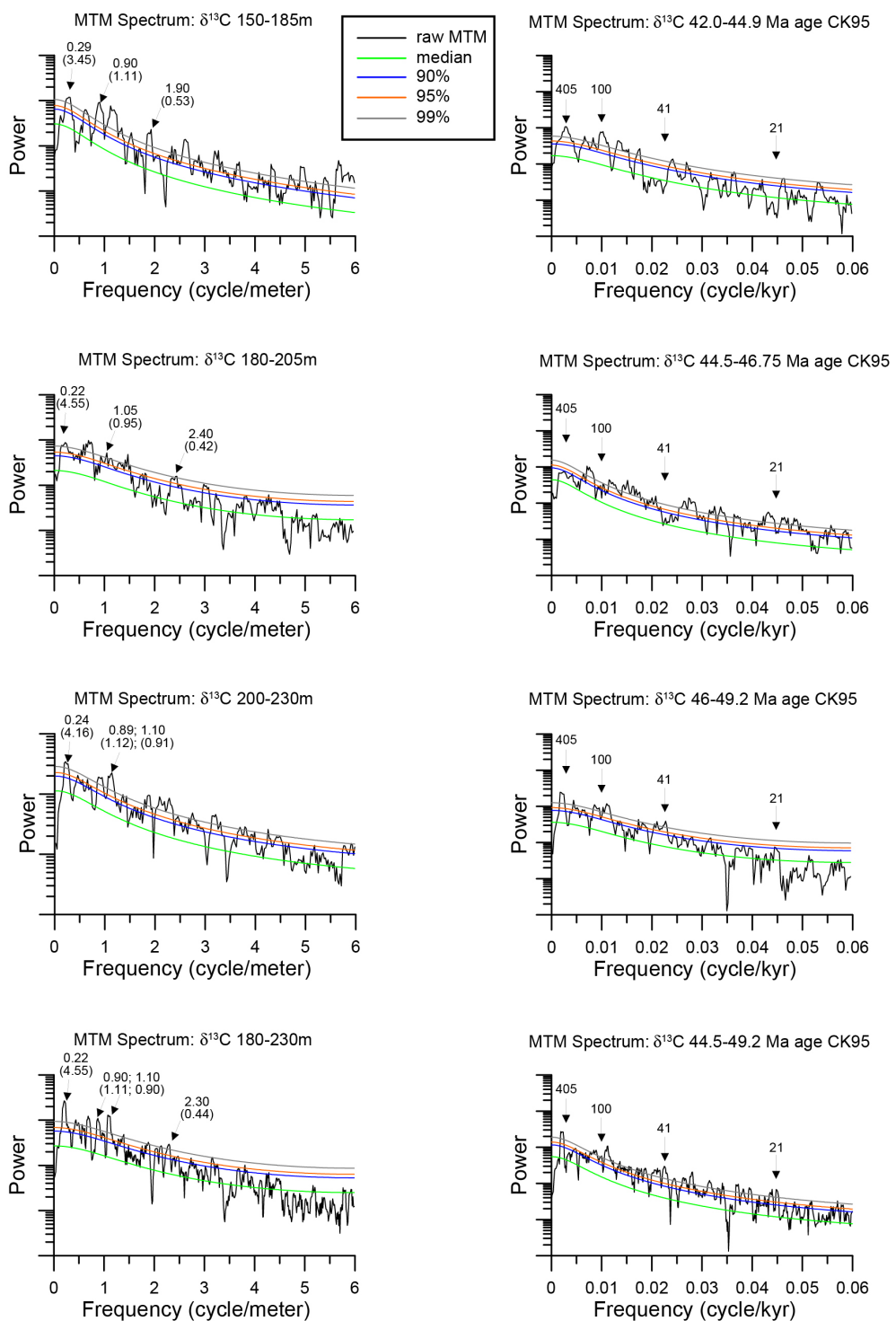
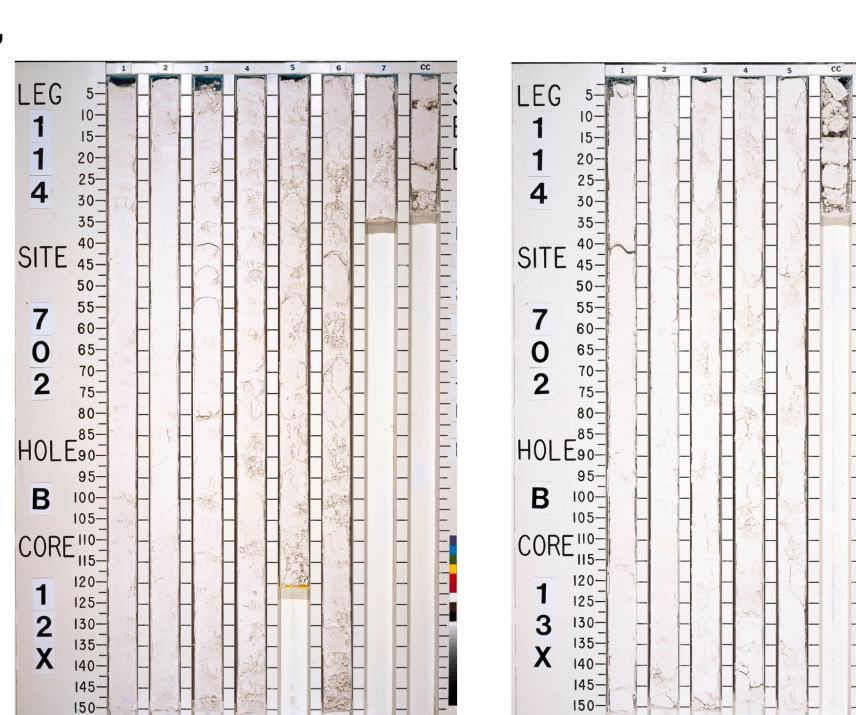
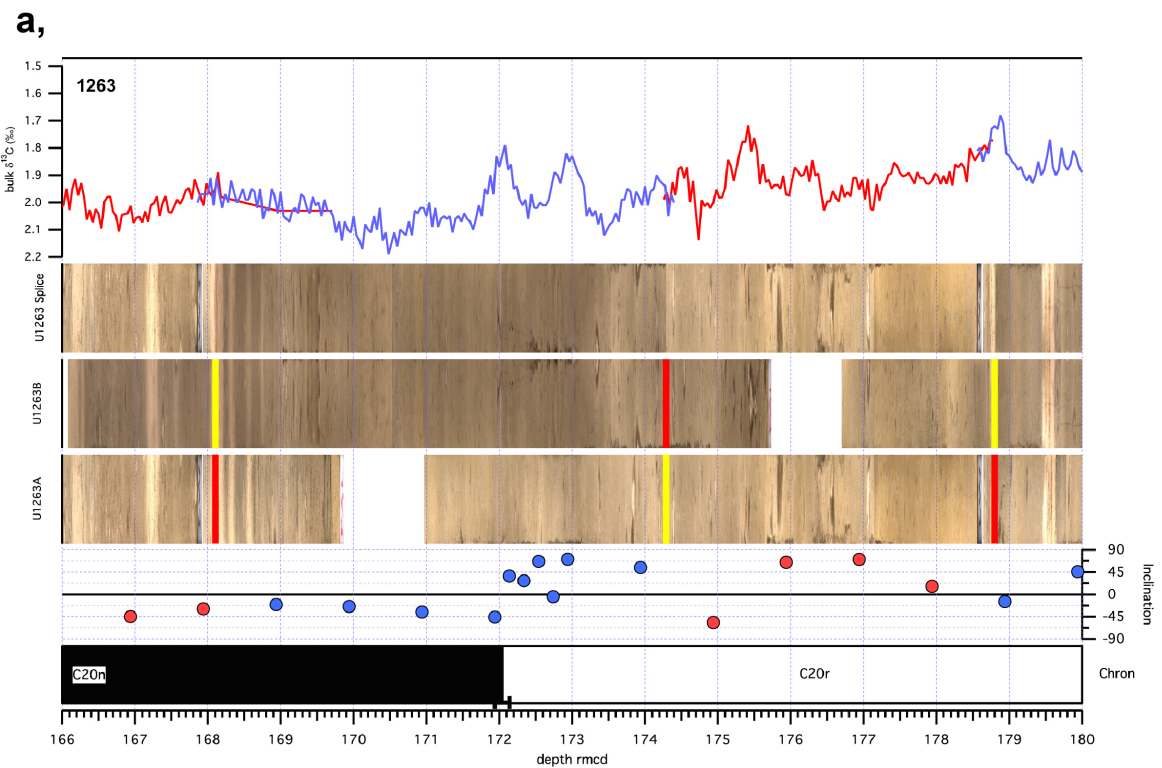
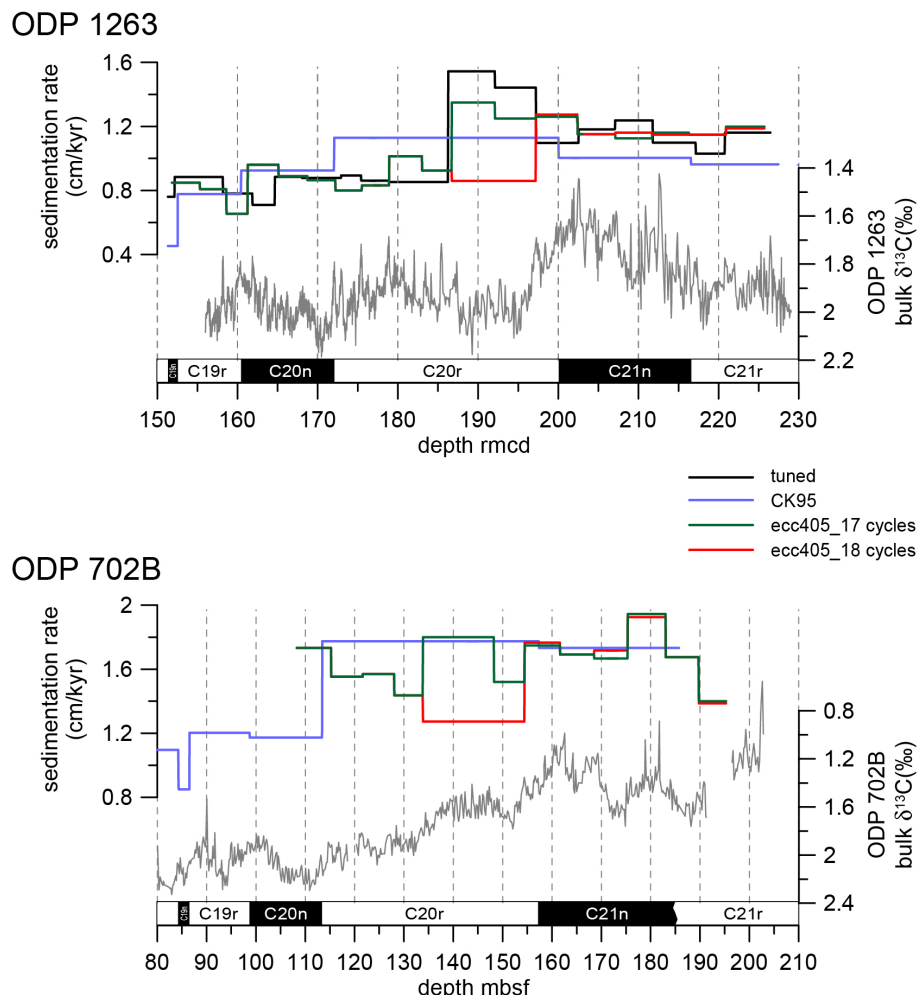


Figure S3



**Figure S4**



**Figure S5**

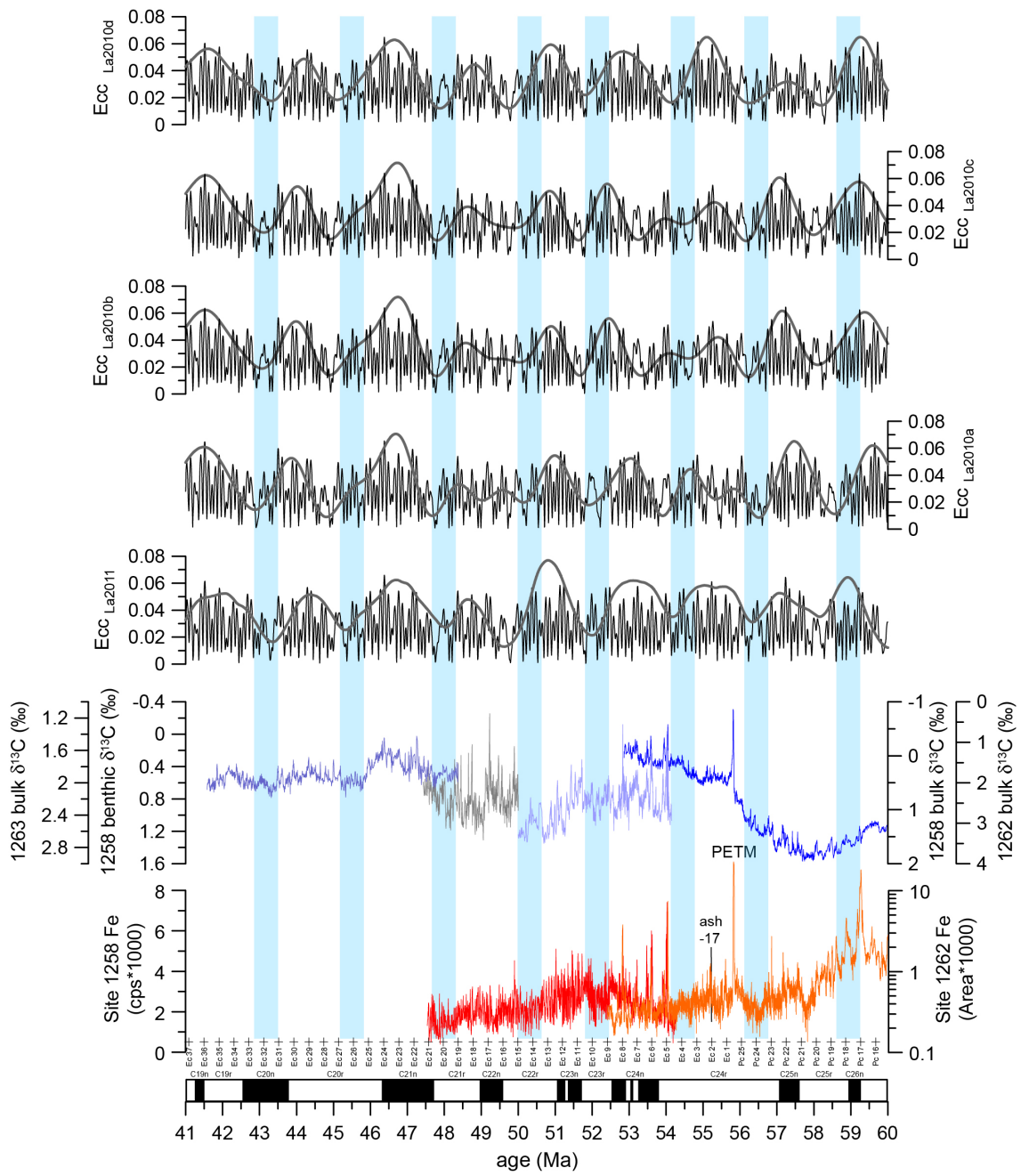


**Figure S6**

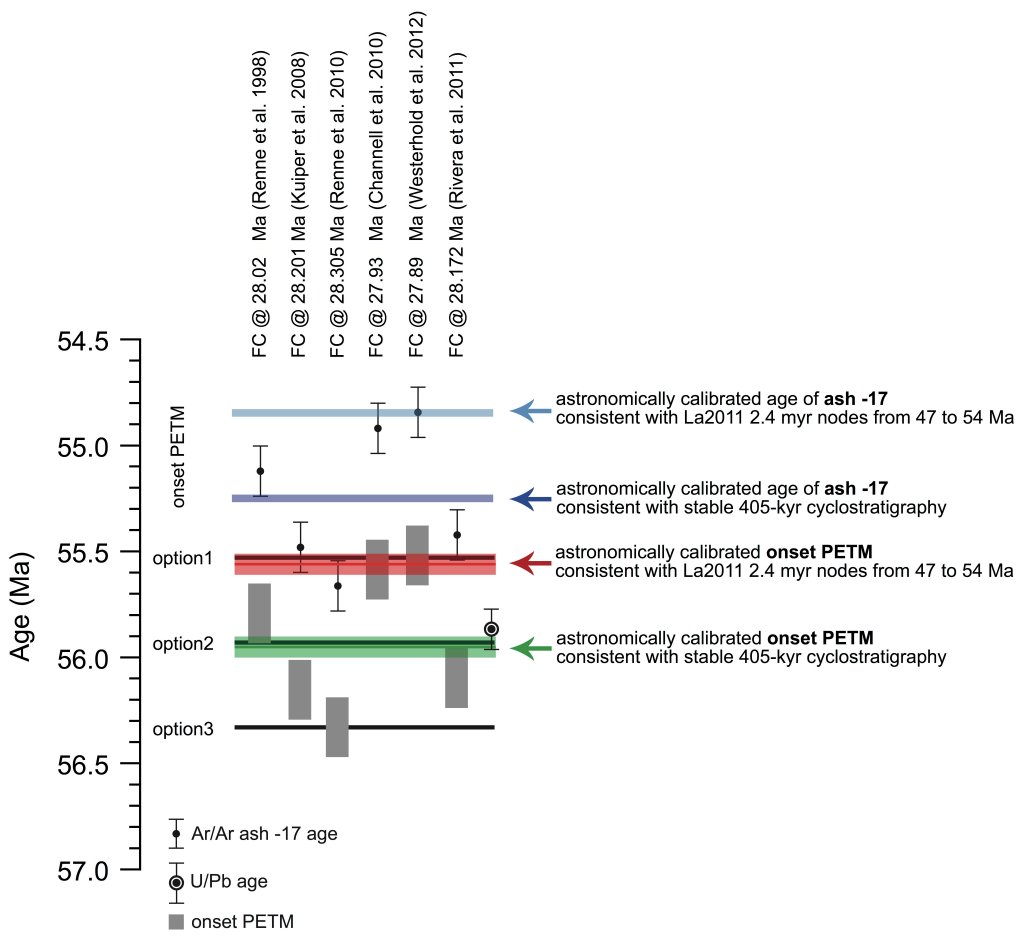


**Figure S7**

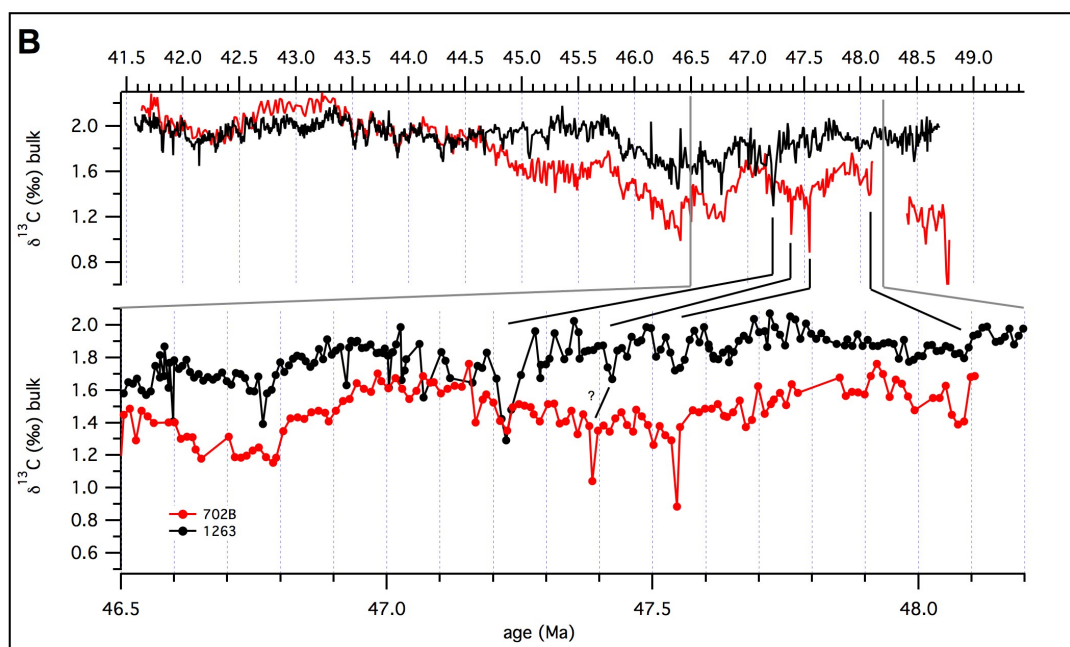
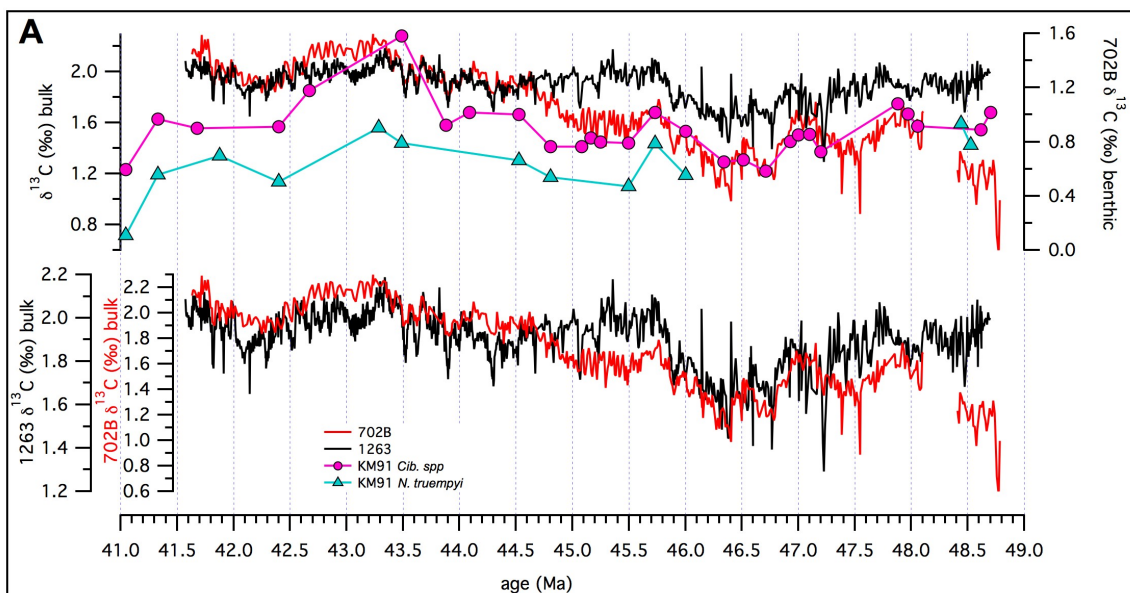


**Figure S8**

## Dataset

### Astronomical Calibration of the Geological Timescale: Closing the Middle Eocene Gap

Thomas Westerhold\*, Ursula Röhl, Thomas Frederichs, Steve M. Bohaty, James C. Zachos

\*email: [twesterhold@marum.de](mailto:twesterhold@marum.de)

The data reported in this paper are open access archived at the Pangaea ([www.pangaea.de](http://www.pangaea.de)) database online at <http://doi.pangaea.de/10.1594/PANGAEA.845986>. This supplement includes tables S4 to S13; extensive tables S1 to S3 are open access available at the links to Pangaea database.

#### Tables:

- Table S1 - Bulk stable isotope data ODP 702B (available [here](#))
- Table S2 - Bulk stable isotope data ODP 1263 (available [here](#))
- Table S3 – ODP 1263 raw inclination, declination, and intensity data for each measurement step (available [here](#))
- Table S4 - Magnetostratigraphy ODP 1263
- Table S5 - Hole 702B and Site 1263 Calcareous Nannofossil datums
- Table S6 - Relative and absolute 405-kyr eccentricity cycle age model for ODP Hole 702B and Site 1263
- Table S7 - Offsets applied to cores from Holes 1263A, 1263B, 1263C
- Table S8 - List of tie points to create the revised composite depth scale (rmcd) for Site 1263
- Table S9 - Paleomagnetic data from ODP 1263
- Table S10 - Astronomical tuning age tie points
- Table S11 - Comparison of magnetochron boundary ages in million years
- Table S12 - Comparison of magnetochron boundary durations in million years
- Table S13 - Comparison of durations of magnetochrons in million years including uncertainties in magnetic anomaly width

**Table S4** Magnetostratigraphy ODP 1263

Chron	Top			Bottom			Mean		
	Site, Hole, Core, Section, Interval (cm)	Depth (mbsf)	Depth (rmcd)	Site, Hole, Core, Section, Interval (cm)	Depth (mbsf)	Depth (rmcd)	Depth (mbsf)	Depth (rmcd)	Error (m)
C20n (y)	1263B-10H-4, 30	136.30	160.34	1263B-10H-4, 50	136.50	160.54	136.40	160.44	± 0.1
C20n (o)	1263B-11H-4, 141	146.91	171.94	1263B-11H-5, 11	147.11	172.14	147.01	172.04	± 0.1
C21n (y)	1263A-19H-5, 108	170.88	199.94	1263B-14H-1, 97	170.47	200.14	170.68	200.04	± 0.1
C21n (o)	1263B-15H-6, 99	185.49	216.34	1263B-15H-6, 39	185.89	216.74	185.69	216.54	± 0.2

**Table S5** Hole 702B and Site 1263 Calcareous Nannofossil datums

Bioevent	Age <sup>s</sup>	Position in <sup>#</sup> Magneto- stratigraphy	Top Core, section interval (cm)	Bottom Core, section interval (cm)	Top Depth (m)	Bottom Depth (m)	Mean Depth (m)	error (±m)
<b>Hole 702B*</b>								
LO R. umbilicus >14µm	43.06	C20n.58	702B11X-5,5	702B11X-5,45	97.85	98.25	98.05	0.20
Site 1263**								
HO <i>Nannotetrina</i> spp.	43.06	C20n.58	1263A15H-CC	1263A16H-1,45	155.27	157.16	156.22	0.94
HO <i>N. fulgens</i> ( <i>alata</i> )	43.72	C20n	1263A15H-CC	1263B11H-4,80	169.84	171.34	170.59	0.75
HO <i>C. gigas</i>	43.96	C20r.93	1263B12H-1,40	1263B12H-1,140	177.09	178.09	177.59	0.50
LO <i>C. gigas</i>	46.11	C20r.06	1263B13H-3,120	1263B13H-4,40	192.38	193.08	192.73	0.35
LO <i>N. fulgens</i> ( <i>alata</i> )	46.80	C21n.68	1263B14H-3,40	1263B14H-3,120	202.58	203.39	202.99	0.40
HO <i>D. lodoensis</i>	48.37	C21r.59	1263A21H-2,40	1263A21H-2,140	215.04	215.56	215.06	0.26

Note: HO = highest occurrence, LO = lowest occurrence; <sup>s</sup>Agnini et al. 2014, <sup>#</sup>Pea 2011, <sup>\*</sup>Shipboard Scientific Party 2004, <sup>#</sup>Position in Magnetochron is from Base of Chron; depth in 702B is mbsf and 1262 is rmcd.

**Table S6** Relative and absolute 405-kyr eccentricity cycle age model for ODP Hole 702B and Site 1263

405-kyr cycle	Site 702B depth (mbsf)	Site 1263 depth (rmcd)	relative age	absolute age	
			(Ma)	405-kyr cycle	La2011 (Ma)
# 1	-	158.60	0.405	# 104	41.904
# 2	-	161.25	0.810	# 105	42.308
# 3	-	165.10	1.215	# 106	42.708
# 4	108.20	168.70	1.620	# 107	43.112
# 5	115.20	172.20	2.025	# 108	43.516
# 6	121.60	175.50	2.430	# 109	43.928
# 7	128.00	178.90	2.835	# 110	44.336
# 8	133.80	183.00	3.240	# 111	44.740
# 9	-	186.70	3.645	# 112	45.140
# 10	148.20	(192.10)	4.050	# 113	45.540
# 11	154.40	197.20	4.455	# 114	45.948
# 12	161.60	202.40	4.860	# 115	46.360
# 13	168.50	207.10	5.265	# 116	46.768
# 14	175.30	211.70	5.670	# 117	47.176
# 15	183.00	216.30	6.075	# 118	47.572
# 16	189.70	220.90	6.480	# 119	47.972
# 17	195.30	225.70	6.885	# 120	48.372

**Table S7** Offsets applied to cores from Holes 1263A, 1263B, 1263C

Core	Offset Ship (m)	Revised Offset (m)	Δ Ship – Revised (m)	Depth		Source
				(mbsf)	(rmcd)	
<b>208-1263A-</b>						
1H	0.00	0.00	0.00	0.00	0.00	ship
2H	0.41	0.41	0.00	2.30	2.71	ship
3H	2.12	2.12	0.00	11.80	13.92	ship
4H	3.83	3.83	0.00	21.30	25.13	ship
5H	3.85	3.85	0.00	30.80	34.65	ship
6H	7.25	7.25	0.00	40.30	47.55	ship
7H	9.11	9.06	0.05	49.80	58.86	this study
8H	10.71	10.11	0.60	59.30	69.41	this study
9H	11.77	11.14	0.63	68.80	79.94	this study
10H	11.79	11.29	0.50	78.30	89.59	this study
11H	13.17	12.67	0.50	87.80	100.47	this study
12H	13.73	13.23	0.50	97.30	110.53	this study
13H	17.53	17.03	0.50	106.80	123.83	this study
14H	17.75	21.03	-3.28	116.30	137.33	this study
15H	20.52	23.73	-3.21	125.80	149.53	this study
16H	21.89	25.13	-3.24	135.30	160.43	this study
17H	23.02	26.34	-3.32	144.80	171.14	this study
18H	23.94	27.44	-3.50	154.30	181.74	this study
19H	25.47	29.06	-3.59	163.80	192.86	this study
20H	27.77	31.36	-3.59	173.30	204.66	this study
21H	30.34	33.83	-3.49	182.80	216.63	this study
22H*	32.34	31.86	0.48	192.30	224.16	this study
23H	32.55	32.55	0.00	201.80	234.35	ship
24H	34.65	34.65	0.00	208.10	242.75	ship
25H	35.85	35.85	0.00	217.60	253.45	ship
26H	36.85	36.85	0.00	222.60	259.45	ship
27H	40.03	40.03	0.00	232.10	272.13	ship
28H	42.52	42.52	0.00	241.60	284.12	ship
29H	43.70	43.78	-0.08	251.10	294.88	W07
30H	45.71	45.79	-0.08	260.60	306.39	W07
31H	46.40	46.48	-0.08	270.10	316.58	W07
32H	48.38	49.08	-0.70	271.60	320.68	W07
33H	51.00	50.60	0.40	281.10	331.70	W07
34X	51.24	50.86	0.38	284.10	334.96	W07
35X	52.36	51.98	0.38	290.30	342.28	W07
36X	54.10	53.72	0.38	300.00	353.72	W07
37X	55.38	55.00	0.38	307.10	362.10	W07
38X	57.11	56.73	0.38	316.70	373.43	W07
39X	58.85	58.47	0.38	326.40	384.87	W07
40X	60.58	60.20	0.38	336.00	396.20	W07
<b>208-1263B-</b>						
1H	7.31	7.30	0.01	46.00	53.30	this study
2H	9.41	9.00	0.41	55.50	64.50	this study
3H	11.04	10.45	0.59	65.00	75.45	this study
4H	12.09	11.43	0.66	74.50	85.93	this study
5H	14.69	14.25	0.44	84.00	98.25	this study
6H	15.64	15.27	0.37	93.50	108.77	this study
7H	16.98	20.32	-3.34	103.00	123.32	this study
8H	18.34	21.57	-3.23	112.50	134.07	this study
9H	19.95	23.23	-3.28	122.00	145.23	this study
10H	20.78	24.04	-3.26	131.50	155.54	this study
11H	21.78	25.03	-3.25	141.00	166.03	this study
12H	22.68	26.20	-3.52	150.50	176.70	this study
13H	24.57	28.17	-3.60	160.00	188.17	this study
14H	26.12	29.67	-3.55	169.50	199.17	this study
15H	27.35	30.85	-3.50	177.00	207.85	this study
16H	29.69	33.13	-3.44	186.50	219.63	this study
17H*	29.69	29.21	0.48	196.00	225.21	this study
18H*	31.11	30.63	0.48	197.20	227.83	this study
19H	32.60	32.60	0.00	201.00	233.60	ship
20H	33.71	33.71	0.00	204.90	238.61	ship
21H	35.92	35.92	0.00	214.40	250.32	ship
22H	38.33	38.33	0.00	223.90	262.23	ship
23H	40.47	40.47	0.00	233.40	273.87	ship

24H	42.29	42.29	0.00	242.90	285.19	ship
25H	42.95	43.03	-0.08	252.40	295.43	W07
26X	44.12	44.20	-0.08	261.90	306.10	W07
27X	47.38	49.28	-1.90	271.10	320.38	W07
28X	50.83	50.58	0.25	280.70	331.28	W07
29X	52.56	52.16	0.40	290.30	342.46	W07
30X	54.30	53.90	0.40	300.00	353.90	W07
31X	56.03	55.63	0.40	309.60	365.23	W07
32X	57.76	57.36	0.40	319.20	376.56	W07
33X	59.51	59.11	0.40	328.90	388.01	W07
<hr/>						
208-1263C-						
1H	13.11	12.72	0.39	90.00	102.72	this study
2H	14.98	17.5	-2.52	99.50	117.00	this study
3H	18.26	21.48	-3.22	109.00	130.48	this study
4H*	32.32	31.84	0.48	193.00	224.84	this study
5H	33.00	33.00	0.00	202.50	235.50	ship
6H	33.83	33.83	0.00	212.00	245.83	ship
7H	34.27	34.27	0.00	221.50	255.77	ship
8H	36.94	36.94	0.00	225.40	262.34	ship
9H	39.79	39.79	0.00	234.90	274.69	ship
10H	41.88	41.88	0.00	244.40	286.28	ship
11H	43.71	43.79	-0.08	253.90	297.69	W07
12H	45.42	45.5	-0.08	263.40	308.90	W07
13H	47.21	47.98	-0.77	272.90	320.88	W07
14H	50.31	49.91	0.40	282.40	332.31	W07
15H	50.31	49.91	0.40	285.60	335.51	W07
16X	50.83	51.08	-0.25	285.70	336.78	W07
<hr/>						
208-1263D-						
1H	46.48	45.76	0.72	272.00	317.76	W07
2H	48.38	47.73	0.65	275.20	322.93	W07
3H	50.61	50.34	0.27	281.50	331.84	W07
4H	50.63	50.30	0.33	284.30	334.60	W07

\* strong core disturbance

---

**Table S8** List of tie points to create the revised composite depth scale (rmcd) for Site 1263

Hole, core, section interval (cm)	Depth		Hole, core, section interval (cm)	Depth		Source	
	(mbsf)	(rmcd)		(mbsf)	(rmcd)		
1263A-1H-2, 50	2.00	2.00	Append to	1263A-2H-1, 0	2.30	2.71	ship
1263A-2H-7, 30	11.60	12.01	Append to	1263A-3H-1, 0	11.80	13.92	ship
1263A-3H-7, 30	21.10	23.22	Append to	1263A-4H-1, 0	21.30	25.13	ship
1263A-4H-7, 35	30.65	34.48	Tie to	1263A-6H-1, 0	40.30	47.55	ship
1263A-6H-5, 12.5	46.425	53.675	Tie to	1263B-1H-1, 37.5	46.375	53.675	this study
1263B-1H-6, 57.5	54.075	61.385	Tie to	1263A-7H-2, 102.5	52.325	61.385	this study
1263A-7H-5, 47.5	56.275	65.345	Tie to	1263B-2H-1, 85	56.35	65.345	this study
1263B-2H-5, 52.5	62.025	71.035	Tie to	1263A-8H-2, 12.5	60.925	71.035	this study
1263A-8H-6, 42.5	67.225	77.345	Tie to	1263B-3H-2, 40	66.90	77.345	this study
1263B-3H-5, 47.5	71.475	81.935	Tie to	1263A-9H-2, 50	70.80	81.935	this study
1263A-9H-7, 7.5	77.375	88.525	Tie to	1263B-4H-2, 110	77.10	88.525	this study
1263B-4H-6, 45	82.45	93.89	Tie to	1263A-10H-3, 130	82.60	93.89	this study
1263A-10H-7, 42.5	87.725	99.025	Tie to	1263B-5H-1, 77.5	84.775	99.025	this study
1263B-5H-7, 17.5	92.705	106.965	Tie to	1263C-1H-3, 125	94.25	106.965	this study
1263C-1H-6, 12.5	97.625	110.37	Tie to	1263B-6H-2, 10	95.10	110.37	this study
1263B-6H-6, 127.5	102.275	117.545	Tie to	1263C-2H-1, 55	100.05	117.545	this study
1263C-2H-7, 6	108.06	125.54	Tie to	1263B-7H-2, 72	105.22	125.54	this study
1263B-7H-6, 137.5	111.875	132.075	Tie to	1263C-3H-2, 10	110.60	132.075	this study
1263C-3H-4, 47.5	113.975	135.465	Tie to	1263B-8H-1, 140	113.90	135.465	this study
1263B-8H-4, 55	117.55	139.13	Tie to	1263A-14H-2, 30	118.10	139.13	this study
1263A-14H-6, 150	123.89	144.93	Append to	1263B-9H-1, 0	122.00	145.23	this study
1263B-9H-4, 115	127.65	150.88	Tie to	1263A-15H-1, 135	127.15	150.88	this study
1263A-15H-5, 40	132.20	155.94	Tie to	1263B-10H-1, 40	131.90	155.94	this study
1263B-10H-5, 30	137.80	161.85	Tie to	1263A-16H-1, 142.5	136.725	161.85	this study
1263A-16H-6, 17.5	142.975	168.105	Tie to	1263B-11H-2, 57.5	143.075	168.105	this study
1263B-11H-6, 75	149.25	174.29	Tie to	1263A-17H-3, 15	147.95	174.29	this study
1263A-17H-6, 15	152.45	178.80	Tie to	1263B-12H-2, 60	152.60	178.80	this study
1263B-12H-6, 80	157.50	183.71	Tie to	1263A-18H-2, 47.5	156.275	183.71	this study
1263A-18H-5, 102.5	161.325	188.765	Tie to	1263B-13H-1, 60	160.60	188.765	this study
1263B-13H-4, 132.5	165.825	194.005	Tie to	1263A-19H-1, 115	164.95	194.005	this study
1263A-19H-5, 102.5	170.825	199.895	Tie to	1263B-14H-1, 72.5	170.225	199.895	this study
1263B-14H-5, 137.5	176.875	206.555	Tie to	1263A-20H-2, 40	175.20	206.555	this study
1263A-20H-5, 70	180.00	211.37	Tie to	1263B-15H-3, 52.5	180.525	211.37	this study
1263B-15H-7, 5	186.05	216.90	Tie to	1263A-21H-1, 27.5	183.075	216.90	this study
1263A-21H-3, 97.5	186.775	220.605	Tie to	1263B-16H-1, 97.5	187.475	220.605	this study
1263B-16H-7, 57.5	196.075	229.215	<b>strong coring disturbance from 229.22 to 233.60</b>				
				1263B-19H-1	201.00	233.60	W07
1263B-19H-3, 8	204.08	236.68	Tie to	1263A-23H-2, 83.5	204.13	236.68	W07
1263A-23H-4, 48	206.76	239.31	Tie to	1263B-20H-1, 70	205.60	239.31	W07
1263B-20H-7, 33	214.22	247.93	Tie to	1263A-24H-4, 67.5	213.28	247.93	W07
1263A-24H-7, 25	217.25	251.90	Tie to	1263B-21H-2, 7.5	215.98	251.90	W07
1263B-21H-5, 103	221.42	257.34	Tie to	1263C-7H-2, 11	223.07	257.34	W07
1263C-7H-4, 15	225.28	259.55	Tie to	1263A-26H-1, 10	222.70	259.55	W07
1263A-26H-3, 120	226.80	263.65	Tie to	1263B-22H-1, 142	225.32	263.65	W07
1263B-22H-7, 65	233.55	271.88	Append to	1263A-27H-1, 0	232.10	272.13	W07
1263A-27H-6, 55	240.15	280.18	Tie to	1263C-9H-4, 98.5	240.39	280.18	W07
1263C-9H-7, 65	244.55	284.34	Tie to	1263A-28H-1, 22.5	241.82	284.34	W07
1263A-28H-3, 78	245.38	287.90	Tie to	1263B-24H-2, 121	245.61	287.90	W07
1263B-24H-6, 20	250.60	292.89	Tie to	1263C-10H-5, 61	251.01	292.89	W07
1263C-10H-7, 122	254.12	296.00	Tie to	1263A-29H-1, 112	252.22	296.00	W07
1263A-29H-5, 120	258.30	302.00	Tie to	1263C-11H-3, 138.5	258.29	302.08	W07
1263C-11H-7, 5	263.35	307.06	Tie to	1263A-30H-1, 75	261.35	307.14	W07
1263A-30H-7, 33	269.92	315.63	Tie to	1263C-12H-5, 81	270.21	315.71	W07
1263C-12H-CC, 28	273.09	318.59	Tie to	1263D-1H-1, 82.5	272.825	318.585	W07
1263D-1H-2, 115	274.65	320.41	Tie to	1263B-27X-1, 3	271.13	320.41	W07
1263B-27X-1, 145	272.55	321.83	Tie to	1263A-32H-1, 115	272.75	321.83	W07
1263A-32H-5, 30	277.90	326.98	Tie to	1263C-13H-5, 10	279.00	326.98	W07
1263C-13H-cc, 10	282.87	330.77	Append to	1263D-3H-1, 0.0	281.50	331.84	R07
1263D-3H-1, 90	282.40	332.74	Tie to	1263C-14H-1, 43	282.83	332.74	R07
1263C-14H-2, 149	285.39	335.30	Tie to	1263D-4H-1, 70	285.00	335.30	R07
1263D-4H-1, 90	285.20	335.50	Tie to	1263A-34X-1, 54	284.64	335.50	R07
1263A-34X-2, 146	287.06	337.92	Tie to	1263C-16X-1, 114	286.84	337.92	R07
1263C-16X-3, 60	288.80	339.88	end of splice				

**Table S9** Paleomagnetic data interpretation from ODP 1263

Site	Hole	Core Type	Section	Section depth (cm)	Depth mbsf	Depth rmcd	Inclination (°)	Declination (°)	MAD (°)	steps used
1263	A	15H	4	91	131.21	154.94	61.9	245.7	3.3	2,3,4,5,6,7,8
1263	B	10H	1	40	131.90	155.94	42.4	159.5	5.9	2,3,4,5,6,7,8
1263	B	10H	1	140	132.90	156.94	52.1	75.2	3.8	2,3,4,5,6,7
1263	B	10H	2	90	133.90	157.94	3.8	11.3	7.1	2,3,4,5,6
1263	B	10H	3	40	134.90	158.94	48.1	32.9	5.0	2,3,4,5,6,7,8
1263	B	10H	3	140	135.90	159.94	80.2	93.3	3.3	2,3,4,5,6
1263	B	10H	4	10	136.10	160.14	56.3	307.5	2.5	2,3,4,5,6,7
1263	B	10H	4	30	136.30	160.34	65.3	43.6	4.2	2,3,4,5,6,7
1263	B	10H	4	50	136.50	160.54	-48.7	279.4	8.4	2,3,4,5,6
1263	B	10H	4	70	136.70	160.74	-64.0	224.3	4.0	2,3,4,5,6,7,8
1263	B	10H	4	90	136.90	160.94	-80.8	272.7	5.2	2,3,4,5,6,7
1263	B	10H	5	40	137.90	161.94	-49.3	223.9	4.9	2,3,4,5,6,7,8
1263	A	16H	2	101	137.81	162.94	-42.4	112.1	5.4	2,3,4,5,6,7,8
1263	A	16H	3	51	138.81	163.94	-37.0	170.3	2.6	2,3,4,5,6,7,8
1263	A	16H	4	1	139.81	164.94	-9.8	160.5	3.1	2,3,4,5,6,7,8
1263	A	16H	4	101	140.81	165.94	-20.8	114.9	5.5	2,3,4,5,6
1263	A	16H	5	51	141.81	166.94	-45.0	155.8	3.0	2,3,4,5,6,7,8
1263	A	16H	6	1	142.81	167.94	-29.2	159.8	2.0	2,3,4,5,6,7,8
1263	B	11H	2	141	143.91	168.94	-20.7	245.0	3.7	2,3,4,5,6
1263	B	11H	3	91	144.91	169.94	-24.4	247.1	4.0	2,3,4,5,6,7
1263	B	11H	4	41	145.91	170.94	-35.8	212.7	1.7	2,3,4,5,6,7,8
1263	B	11H	4	141	146.91	171.94	-46.2	161.1	5.0	3,4,5,6,7,8
1263	B	11H	5	11	147.11	172.14	37.0	189.3	5.8	2,3,4,5,6
1263	B	11H	5	31	147.31	172.34	27.5	259.2	4.7	3,4,5,6
1263	B	11H	5	51	147.51	172.54	66.6	269.7	4.2	2,3,4,5,6,7
1263	B	11H	5	71	147.71	172.74	-4.7	213.8	5.6	2,3,4,5,6,7
1263	B	11H	5	91	147.91	172.94	71.0	134.7	2.1	3,4,5,6,7
1263	B	11H	6	41	148.91	173.94	54.2	117.2	7.2	2,3,4,5,6
1263	A	17H	3	80	148.60	174.94	-56.9	3.2	6.7	2,3,4
1263	A	17H	4	30	149.60	175.94	64.8	341.3	3.4	2,3,4,5,6
1263	A	17H	4	130	150.60	176.94	70.8	312.5	3.5	2,3,4,5,6,7,8
1263	A	17H	5	80	151.60	177.94	16.3	315.3	5.0	2,3,4,5,6
1263	B	12H	2	74	152.74	178.94	-14.7	296.4	5.1	4,5,6,7
1263	B	12H	3	24	153.74	179.94	45.8	23.4	6.6	2,3,4,5,6
1263	B	12H	4	39	154.74	180.94	14.3	313.8	3.7	2,3,4,5,6,7,8
1263	B	12H	5	54	155.74	181.94	-9.3	53.9	1.6	4,5,6,7,
1263	B	12H	6	4	156.74	182.94	12.8	295.3	1.5	2,3,4,5,6,7,8,
1263	A	18H	2	70	180.44	183.94	86.5	228.4	4.4	2,3,4,5,6,7,8,
1263	A	18H	3	20	181.44	184.94	79.6	140.7	3.5	2,3,4,5,6,7,8,
1263	A	18H	3	120	182.44	185.94	53.2	145.5	2.5	2,3,4,5,6,7,
1263	A	18H	4	70	183.44	186.94	73.0	51.2	3.7	2,3,4,5,6,7,8,
1263	A	18H	5	20	184.44	187.94	72.8	122.2	2.4	2,3,4,5,6,7,8,
1263	B	13H	1	77	160.77	188.94	82.6	339.8	2.3	2,3,4,5,6,7,8,
1263	B	13H	2	27	161.77	189.94	62.9	131.6	2.6	2,3,4,5,6,7,
1263	B	13H	2	127	162.77	190.94	44.0	147.8	5.5	2,3,4,5,6,7,
1263	B	13H	3	77	163.77	191.94	47.8	121.9	2.3	2,3,4,5,6,7,8,
1263	B	13H	4	27	164.77	192.94	49.2	146.5	5.5	3,4,5,6,7,
1263	B	13H	4	127	165.77	193.94	69.4	253.3	6.6	2,3,4,5,6,7,
1263	A	19H	2	58	165.88	194.94	29.7	225.4	4.3	2,3,4,5,6,
1263	A	19H	3	8	166.88	195.94	53.4	296.0	3.7	2,3,4,5,6,7,8,
1263	A	19H	3	108	167.88	196.94	49.1	141.1	4.8	3,4,5,6,
1263	A	19H	4	58	168.88	197.94	28.1	159.4	4.1	2,3,4,5,6,7,8,
1263	A	19H	5	8	169.88	198.94	47.5	321.9	4.6	2,3,4,5,6,
1263	A	19H	5	108	170.88	199.94	35.4	355.1	3.8	2,3,4,5,
1263	B	14H	1	77	170.27	199.94	39.6	305.4	3.8	2,3,4,5,
1263	B	14H	1	97	170.47	200.14	-43.5	259.1	6.0	2,3,4,5,6,7,8
1263	B	14H	1	117	170.67	200.34	-22.4	238.1	8.9	3,4,5,6
1263	B	14H	1	137	170.87	200.54	-9.4	279.2	5.3	4,5,6
1263	B	14H	2	7	171.02	200.74	-29.7	259.5	5.4	2,3,4,5,6
1263	B	14H	2	27	171.26	200.94	-28.6	249.0	8.1	4,5,6
1263	B	14H	2	47	171.47	201.14	-82.1	270.8	1.5	2,3,4,5,6
1263	B	14H	2	127	172.27	201.94	-67.0	300.2	5.1	3,4,5,6,7
1263	B	14H	3	77	173.27	202.94	23.8	305.1	6.3	2,3,4,5,6,7,8
1263	B	14H	4	27	174.27	203.94	-57.7	301.9	3.5	2,3,4,5,6
1263	B	14H	4	127	175.27	204.94	-32.9	344.6	5.9	4,5,6,7
1263	B	14H	5	77	176.27	205.94	-74.0	315.8	3.4	4,5,6,7,8
1263	A	20H	2	78	175.58	206.94	-18.0	238.8	1.8	2,3,4,5,6,7

1263	A	20H	3	28	176.58	207.94	10.3	212.4	7.4	2,3,4,5,6
1263	A	20H	3	128	177.58	208.94	-0.4	256.3	2.4	4,5,6,7
1263	A	20H	4	78	178.58	209.94	8.7	238.2	2.4	2,3,4,5,6,7,8
1263	B	15H	3	20	180.20	211.05	-40.4	143.9	2.7	2,3,4,5,6,7,8
1263	B	15H	3	109	181.09	211.94	-8.7	124.4	2.0	2,3,4,5,6,7,8
1263	B	15H	4	59	182.09	212.94	-18.5	216.9	6.4	2,3,4,5,6,7
1263	B	15H	5	9	183.09	213.94	-15.7	147.0	3.8	2,3,4,5,6,7,8
1263	B	15H	5	109	184.09	214.94	-36.7	146.0	3.8	2,3,4,5,6,7,8
1263	B	15H	6	39	184.89	215.74	-46.0	169.5	1.1	2,3,4,5,6,7,8
1263	B	15H	6	59	185.09	215.94	-44.8	158.5	4.7	2,3,4,5,6,7,8
1263	B	15H	6	79	185.29	216.14	-36.7	158.3	2.2	2,3,4,5,6,7,8
1263	B	15H	6	99	185.49	216.34	-12.0	155.1	2.7	3,4,5,6,7
1263	B	15H	6	119	185.69	216.54	-6.9	147.6	2.1	3,4,5,6
1263	B	15H	6	139	185.89	216.74	16.5	170.6	3.6	2,3,4,5,6
1263	B	15H	7	9	186.09	216.94	5.7	169.8	1.2	4,5,6,7
1263	A	21H	1	31	183.11	216.94	11.9	260.4	2.3	2,3,4,5,6
1263	B	15H	7	29	186.29	217.14	-25.3	145.5	4.5	2,3,4,5,6
1263	B	15H	7	49	186.49	217.34	-12.7	148.6	6.1	2,3,4,5,6,7
1263	A	21H	1	131	184.11	217.94	46.6	251.3	3.1	2,3,4,5,6,7
1263	A	21H	2	81	185.11	218.94	10.0	1.0	2.7	2,3,4,5
1263	A	21H	3	31	186.11	219.94	2.5	272.8	3.1	3,4,5,6,7
1263	A	21H	3	131	187.11	220.94	70.8	203.5	4.5	2,3,4,5,6,7
1263	A	21H	4	81	188.11	221.94	52.3	37.0	2.6	3,4,5
1263	A	21H	5	31	189.11	222.94	12.0	274.6	2.1	3,4,5,6,7,8
1263	A	21H	5	131	190.11	223.94	57.3	2.8	3.8	2,3,4,5,6
1263	A	21H	6	81	191.11	224.94	63.9	87.7	9.0	2,3,4,5
1263	B	16H	5	31	192.81	225.94	32.0	15.5	8.4	2,3,4,5,6,7,8
1263	B	16H	5	131	193.81	226.94	66.1	62.1	3.1	2,3,4,5,6,7
1263	B	16H	6	15	194.15	227.28	-1.6	153.2	4.9	3,4,5,6,7
1263	B	16H	6	50	194.50	227.63	-9.2	191.4	5.5	4,5,6,7
1263	B	16H	6	81	194.81	227.94	-49.0	168.0	6.2	3,4,5
1263	B	16H	6	137	195.37	228.50	-35.2	192.0	6.8	3,4,5,6,7
1263	B	16H	7	35	195.85	228.98	3.7	0.9	9.0	3,4,5,6

**Table S10** Astronomical tuning age tie points

ODP 1263		ODP 702B	
depth (rmcd)	Age La2011 (Ma)	depth (mbsf)	Age La2011 (Ma)
150.69	40.945968	91.69	41.621043
152.14	41.136030	94.92	41.818290
158.17	41.816454	98.23	42.083093
161.86	42.287809	103.22	42.513360
164.64	42.679338	112.04	43.344957
168.04	43.063264	115.02	43.522767
172.93	43.618246	116.70	43.619268
175.41	43.895737	121.26	43.894984
178.85	44.294868	126.92	44.293018
186.25	45.161553	133.80	44.740000
192.10	45.540000	148.20	45.540000
197.23	45.895194	154.36	45.898210
202.53	46.377953	162.16	46.381028
207.07	46.761879	168.83	46.757840
211.77	47.142004	175.94	47.225596
217.13	47.628564	181.74	47.545265
220.76	47.981547	190.89	48.082781
226.47	48.472441		

**Table S11** Comparison of magnetochron boundary ages in million years

Chron	standard GPTS			tuned			tuned – this study <sup>†</sup>		
	CK95	GPTS 2004	GPTS 2012	PEAT Sites <sup>#</sup>	Contessa Hyw	ODP Site 1260	ODP Site 1258 opt.2	ODP Site 1263	ODP Site 702B
C18n.2n (o)	40.130	39.464	40.145	40.076 ± 5	40.120				
C19n (y)	41.257	40.439	41.154	41.075 ± 7	41.250	41.061 ± 9		41.030 ± 13	
C19n (o)	41.521	40.671	41.390	41.306 ± 5	41.510	41.261 ± 4		41.180 ± 11	
C20n (y)	42.536	41.590	42.301	42.188 ± 15	42.540	42.152 ± 7		42.107 ± 13	42.124 ± 4
C20n (o)	43.789	42.774	43.432		43.790	43.449 ± 18		43.517 ± 11	43.426 ± 3
C21n (y)	46.264	45.346	45.724		46.310			46.151 ± 9	46.080 ± 3
C21n (o)	47.906	47.235	47.349				47.723 ± 118	47.575 ± 18	
C22n (y)	49.037	48.599	48.566				48.954 ± 16		
C22n (o)	49.714	49.427	49.344				49.593 ± 42		
C23n.1n (y)	50.778	50.730	50.628				51.051 ± 21		
C23n.1n (o)	50.946	50.932	50.835				51.273 ± 39		
C23n.2n (y)	51.047	51.057	50.961				51.344 ± 32		
C23n.2n (o)	51.743	51.901	51.833				51.721 ± 23		
C24n.1n (y)	52.364	52.648	52.620				52.525 ± 23		
C24n.1n (o)	52.663	53.004	53.074				52.915 ± 29		
C24n.2n (y)	52.757	53.116	53.199				53.037		
C24n.2n (o)	52.801	53.167	53.274				53.111		
C24n.3n (y)	52.903	53.286	53.416				53.249 ± 17		
C24n.3n (o)	53.347	53.808	53.983				53.806 ± 20		

<sup>†</sup>tuned to the orbital solution La2011 (Laskar et al. 2011)<sup>#</sup>combined ages based on Pacific Equatorial Age Transect Sites 1218, U1333 and U1334 (Westerhold et al. 2014)**Table S12** Comparison of magnetochron boundary durations in million years

Chron	standard GPTS			tuned			tuned – this study <sup>†</sup>		
	CK95	GPTS 2004	GPTS 2012	PEAT Sites <sup>#</sup>	Contessa Hyw	ODP Site 1260	ODP Site 1258 opt.2	ODP Site 1263	ODP Site 702B
C18n.2r	1.127	0.975	1.009	0.999 ± 12					
C19n	0.264	0.232	0.236	0.231 ± 12	0.260	0.200 ± 7		0.150 ± 24	
C19r	1.015	0.919	0.911	0.882 ± 20	1.030	0.891 ± 6		0.927 ± 24	
C20n	1.253	1.184	1.131		1.250	1.297 ± 13		1.410 ± 24	1.302 ± 7
C20r	2.475	2.572	2.292		2.520			2.634 ± 20	2.654 ± 6
C21n	1.642	1.889	1.625				1.424 ± 27		
C21r	1.131	1.364	1.217				1.231 ± 134		
C22n	0.677	0.828	0.778				0.639 ± 58		
C22r	1.064	1.303	1.284				1.458 ± 63		
C23n.1n	0.168	0.202	0.207				0.222 ± 60		
C23n.1r	0.101	0.125	0.126				0.071 ± 71		
C23n.2n	0.696	0.844	0.872				0.377 ± 55		
C23n.2r	0.621	0.747	0.787				0.804 ± 46		
C24n.1n	0.299	0.356	0.454				0.390 ± 52		
C24n.1r	0.094	0.112	0.125				0.122		
C24n.2n	0.044	0.051	0.075				0.074		
C24n.2r	0.102	0.119	0.142				0.138		
C24n.3n	0.444	0.522	0.567				0.557 ± 37		

<sup>†</sup>tuned to the orbital solution La2011 (Laskar et al. 2011)<sup>#</sup>combined ages based on Pacific Equatorial Age Transect Sites 1218, U1333 and U1334 (Westerhold et al. 2014)**Table S13.** Comparison of durations of magnetochrons in million years including uncertainties in magnetic anomaly width

Chron	CK95		GPTS2004		GPTS2012		this study		Source Site
	min	max	min	max	min	max	min	max	
C19	1.197	1.360	1.069	1.232	1.066	1.228	1.074	1.106	ODP 1260 <sup>*</sup>
C20n	1.172	1.334	1.103	1.266	1.050	1.212	1.273	1.323	ODP 1260 <sup>*</sup>
C20r	2.324	2.626	2.420	2.723	2.141	2.443	2.675	2.729	ODP 1260 <sup>*</sup> , 1263 <sup>#</sup>
C21n	1.506	1.778	1.753	2.026	1.489	1.761	1.397	1.451	ODP 1263 <sup>#</sup>
C21r	0.975	1.287	1.209	1.520	1.061	1.373	1.345	1.413	ODP 1258 <sup>\$</sup>
C22n	0.615	0.739	0.765	0.890	0.716	0.840	0.581	0.697	ODP 1258 <sup>\$</sup>
C22r	0.911	1.217	1.150	1.456	1.131	1.437	1.395	1.521	ODP 1258 <sup>\$</sup>
C23	1.241	1.931	1.574	2.263	1.647	2.337	1.430	1.518	ODP 1258 <sup>\$</sup>
C24	3.119	3.961	3.596	4.438	4.060	4.902	4.492	4.558	ODP 1258 <sup>\$</sup> , 1262 <sup>**</sup>

<sup>\*</sup>Westerhold & Röhl (2013); <sup>#</sup>this study; <sup>\$</sup>Westerhold & Röhl (2009), <sup>\*\*</sup>Westerhold et al. (2007; option 2)

Note: minimum and maximum durations for CK95, GPTS2004 and GPTS2012 are based on the error given for the mean width of magnetic anomalies as published in table 4 of Cande &amp; Kent (1992)